Designing plasmonic systems using optical coupling between nanoparticles

T. J. Davis,[1,2] K. C. Vernon,[1] and D. E. Gómez[1]
[1]*Division of Materials Science and Engineering, CSIRO, Private Bag 33, Clayton Victoria 3168, Australia*
[2]*School of Physics, Monash University, Victoria 3800, Australia*

(Received 7 January 2009; revised manuscript received 14 March 2009; published 15 April 2009)

A theory of the coupling of evanescent optical fields between metallic nanoparticles is developed to provide a basis for designing plasmonic systems. The interaction between metallic nanoparticles is investigated using an electrostatic approximation that describes the localized surface-plasmon resonances for particles much smaller than the wavelength of the exciting radiation. A coupling coefficient is derived relating the surface charge on one particle to the induced surface dipoles on another. The effect of dipole radiation damping is included to model the radiation broadening of the plasmon resonances. The theory enables an analysis of the key factors that control the coupling and that lead to resonances of the particle system. It is shown that the coupling between a simple pair of particles, in the form of stripes, leads to frequency splitting and the formation of a dark mode. The dark mode is associated with little scattering of light but large evanescent electric fields. It is shown that the dark mode has low radiation damping compared to an associated bright mode. The theory can be applied to an arbitrary number of interacting particles, allowing them to be configured to achieve the desired properties of the plasmonic system.

DOI: 10.1103/PhysRevB.79.155423 PACS number(s): 78.67.Bf, 73.20.Mf, 78.20.Bh

I. INTRODUCTION

Plasmonic systems have received much interest in recent years due to their ability to guide, manipulate and enhance light fields on the nanoscale. The design of structures capable of producing strong near-fields has become an active area of plasmonics research with applications in highly sensitive sensor technology,[1–6] surface-enhanced Raman scattering (SERS),[2,7–20] plasmon solar cells,[21–26] and near-field microscopy.[2,14,16,27,28]

Plasmonic substrates need to be carefully designed to produce sharp resonances which enhance the light field and minimize losses. Strong local-field enhancement leads to enhanced nonlinearity which is important for SERS, whereas sharp resonances can lead to high sensitivity to local refractive index changes, both effects enabling chemical sensing at low concentrations. Most plasmonic substrate designs require laying metallic nanoparticles on a surface,[8,9,13,19] using random fractal surfaces,[8,9,15,17] or using gaps between lithographically designed particles ("hot spots").[8,9] Although it is now possible to create a myriad of different nanoscale surface structures, there is still a lack of knowledge over what kinds of surfaces lead to maximal field enhancement and high sensitivity[8,9] and what are the most important factors in surface design for a SERS substrate, sensor device, or solar cell panel.

Normally, field enhancement is hindered by two major factors—radiative damping and resistive losses. The latter is a property of the material, while the former depends on the induced dipole (and to a lesser extent multipole) fields of the particle, which can be controlled with careful design of geometries.

During the analysis of a random substrate using a near-field microscopy probe, Stockman *et al.*[17] found it was possible to stimulate two types of plasmon modes. One of the modes exhibited strongly radiating fields, while the other did not. The first mode was termed a luminous mode, while the latter was termed a dark mode due to the lack of re-radiation. Mechanisms for coupling light into dark modes and the actual purposeful design of dark mode structures is still an active field in plasmonics research, with one of the aims being to obtain strong near-fields for sensing. It has been suggested that dark modes cannot be excited efficiently using an incident field but may be excited by nearby radiative particles.[29] In simulations by Zhang and colleagues, a nearby radiative particle strongly couples to the incident light and to the nonradiative particle, producing electromagnetic induced transparency (EIT).[29] There are many other geometries used to create EIT, with applications in cloaking, improvement of laser beam transmission, new optoelectronic devices, and elimination of self-focusing and self-defocusing effects.[30–36] The work of Zhang and colleagues outlines the basic principle of not only EIT but also stimulation of dark modes, however it does not provide any experimental evidence or investigate/discuss the key design elements for creating plasmonic structures capable of supporting dark modes.[29] The stimulation of strong near-fields for sensing applications was not discussed.

In this paper we investigate the key design parameters for creating resonant plasmonic structures. This is done by extending the work of Mayergoyz *et al.*[37–39] on the electrostatic resonances of nanoparticles, also known as the nonretarded boundary element method (BEM),[40–44] to include the effects of interparticle coupling and radiation losses. The key result is an analytical expression for the electric field distribution of an ensemble (or collection) of particles that depends on the parameters describing each particle (shape, material, surface, and dipole charge distribution) and their geometrical distribution (interparticle distances and relative orientations).

Studies of the electromagnetic coupling between metallic nanostructures have been of some interest in the formation of strong electric fields between metallic nanoparticle dimers for SERS (Ref. 45) and in the optically induced forces for the manipulation of plasmonic nanoparticles,[46–48] both of which are affected by the proximity of one particle to an-

other. While there have been theoretical treatments of the interactions between dielectric particles, such as the multipole expansion method,[49] our particular focus is on nanostructures exhibiting localized surface plasmons. The electrostatic approximation allows us to represent the interactions based on the natural plasmonic resonances (eigenmodes) of the metallic nanostructures which make the formalism applicable to arbitrary shapes. This leads to relatively simple relationships for the coupling between nanostructures which are important for enabling us to design or analyze plasmonic systems.

This paper is organized as follows: in Sec. II we review the main results of the electrostatic approximation that allows a calculation of the collective resonant modes of an ensemble of nanoparticles. The effect of radiation damping is important and is included in the formulation. In Sec. III the formalism is modified to show explicitly the interactions and coupling between all the particles in the ensemble, including radiation damping. This leads to an expression for the coupling coefficient describing the effect of the electric field from one particle on the charge distribution of another. The consequences of this coupling are investigated in Sec. IV with a simple two-particle system. It is shown that the coupling leads to the formation of symmetric and antisymmetric modes, the latter exhibiting the properties of a dark mode.

II. ELECTROSTATIC RESONANCES OF PARTICLES

In this section we discuss the calculation of the electrostatic resonances associated with metallic nanoparticles that are much smaller than the wavelength of the exciting radiation, i.e., the electrostatic approximation which is valid for

$$\varepsilon_b(2\pi d/\lambda)^2 \ll 1, \tag{1}$$

where λ is the vacuum wavelength, ε_b is the electric permittivity of the background medium, and d is the average diameter of the particle system.[3,37–39,42] Since the excitation wavelength is large compared to the system size, the fields within the particle and in the surroundings oscillate with approximately the same phase, so that at any moment of time the particle field appears electrostatic.[37] This approximation begins to fail when there are significant phase delays between different parts of the structure, and this is related to its characteristic size d. The failure occurs when condition (1) is no longer valid which expresses the square of the relative phase shift in radians across the nanostructure. It must be borne in mind that while the electrostatic theory provides a useful guide to resonances and associated effects, for larger structures the values calculated using the electrostatic theory will deviate from the true values so that exact methods, such as BEM, are required for precise calculations. A useful discussion of this issue is given in Ref. 42. We begin by reviewing the theory for an individual particle, which is also valid for an ensemble, and we then include the effects of radiation damping.

A. Electrostatic approximation

The electromagnetic field surrounding a particle can be determined by solving for the self-sustained distribution of surface charge $\sigma(\mathbf{r})$ or surface dipoles $\tau(\mathbf{r})$ across the surface of the nanoparticle. At a given point on the surface of a particle q, the surface charge is the source of an electric field that induces electric charges at all other points across the surface. The equation linking the induced charge at $\mathbf{r}$ with all charges distributed over the surface $\mathbf{r}_q$ is given by[37]

$$\sigma(\mathbf{r}) = \frac{\gamma_q}{2\pi}\oint \sigma(\mathbf{r}_q)\frac{(\mathbf{r}-\mathbf{r}_q)\cdot\hat{\mathbf{n}}}{|\mathbf{r}-\mathbf{r}_q|^3}dS_q, \tag{2}$$

with $\hat{\mathbf{n}}$ the surface normal at $\mathbf{r}$ and

$$\gamma_q = \frac{\varepsilon_q - \varepsilon_b}{\varepsilon_q + \varepsilon_b}, \tag{3}$$

where ε_q is the electric permittivity of the particle and ε_b is the electric permittivity of the background medium. The parameter γ_q is the eigenvalue associated with the eigenvalue equation Eq. (2). For a given particle geometry γ_q takes on a large number of discrete values γ_q^k, each one corresponding to a particular resonant mode and to a surface charge density $\sigma_q^k(\mathbf{r})$. For a given mode, γ_q is known and once the background permittivity is chosen, then Eq. (3) fixes the permittivity ε_q which in turn fixes the resonant frequency of the particle. It has been shown[37] that valid source-free resonances occur for $\gamma_q > 1$ which, through Eq. (3), requires that $\varepsilon_q < 0$. This permittivity is obtained with metals at frequencies below the bulk plasma frequency so that the resonant modes are identified with localized surface plasmons.

A similar eigenvalue equation can be obtained for the surface dipole distribution

$$\tau(\mathbf{r}) = \frac{\gamma_q}{2\pi}\oint \tau(\mathbf{r}_q)\frac{(\mathbf{r}_q-\mathbf{r})\cdot\hat{\mathbf{n}}_q}{|\mathbf{r}-\mathbf{r}_q|^3}dS_q, \tag{4}$$

where γ_q simultaneously satisfies Eq. (2) and (4). Neither eigenfunctions $\sigma_q^k(\mathbf{r})$ nor $\tau_q^k(\mathbf{r})$ associated with a particular set of eigenvalues γ_q^k form an orthogonal set of functions. However, they form a biorthogonal set that obeys the relationship

$$\oint \sigma_q^j(\mathbf{r})\tau_q^k(\mathbf{r})dS = \delta^{jk}. \tag{5}$$

As a consequence there is an ambiguity in the scaling of the functions because any eigenfunction can be multiplied by a constant factor f and its adjoint function multiplied by $1/f$ so that Eq. (5) is still obeyed. This ambiguity is also true for the relationship between the particle resonance and the size of the nanoparticle. As long as the ratio of the particle dimensions remains the same (regardless of size) the resonance permittivity ε_q remains the same.[37] This is a key feature of the electrostatic approximation.

An external electric field, oscillating with angular frequency ω, applied to a nanoparticle, excites a surface charge distribution $\sigma(\mathbf{r},\omega)$ that can be represented by a superposition of the surface charge eigenmodes $\sigma_q^k(\mathbf{r})$ (Ref. 39)

$$\sigma(\mathbf{r},\omega) = \sum_k a_q^k(\omega)\sigma_q^k(\mathbf{r}). \tag{6}$$

The frequency-dependent coefficient $a_q^k(\omega)$ in the expansion is related to the strength of the applied field that is exciting the resonance and, according to Mayergoyz *et al.*,[39] it is given by

$$a_q^k = \frac{(\varepsilon_q - \varepsilon_b)(\varepsilon_q^k - \varepsilon_b)}{\varepsilon_q^k - \varepsilon_q}\mathbf{E}_0 \cdot \oint \hat{\mathbf{n}}\tau_q^k(\mathbf{r}_q)dS_q. \tag{7}$$

The applied field $\mathbf{E}_0$ has been taken out of the integration since according to the electrostatic approximation, it is constant across the particle. ε_q is the complex permittivity of the nanoparticle at the particular excitation frequency while ε_q^k represents the real part of ε_q for the kth resonance.

By defining a vector

$$\mathbf{b}_q^k = \frac{(\varepsilon_q - \varepsilon_b)(\varepsilon_q^k - \varepsilon_b)}{\varepsilon_q^k - \varepsilon_q}\oint \hat{\mathbf{n}}\tau_q^k(\mathbf{r}_q)dS_q, \tag{8}$$

the expansion coefficient is simply given by

$$a_q^k = \mathbf{b}_q^k \cdot \mathbf{E}_0. \tag{9}$$

This coefficient describes the contribution to the total surface charge [Eq. (6)] by the kth resonant mode induced by an applied field. Implicit in this description is a time dependence of the applied field with a form $\exp(-i\omega t)$.

B. Radiation damping

A particle interacting with an applied electric field reradiates or scatters radiation into the surrounding environment. Associated with this is a damping factor that limits the strength of the resonance. Although the general form of the electrostatic interaction between a particle and an applied electromagnetic field can be written down in terms of multipoles, the dominant radiation is from the oscillating dipole moment of the particle. While higher-order multipoles can be included, for simplicity we model only the dipole radiation effects which requires an expression for the dipole moment. For a particle q, the dipole moment is given by

$$\mathbf{p} = \oint \mathbf{r}\sigma(\mathbf{r})dS = \oint \sum_k a_q^k \mathbf{r}\sigma_q^k(\mathbf{r})dS = \sum_k \mathbf{p}_q^k(\mathbf{b}_q^k \cdot \mathbf{E}_0). \tag{10}$$

Note that the scalar product is between the vector $\mathbf{b}_q^k$ and the applied electric field. A more useful expression is obtained by writing the two eigenfunction terms as a dyadic

$$\vec{\boldsymbol{\chi}} = \sum_k \mathbf{p}_q^k \mathbf{b}_q^k, \tag{11}$$

then the induced dipole moment is given by the familiar expression

$$\mathbf{p} = \vec{\boldsymbol{\chi}} \cdot \mathbf{E}_0. \tag{12}$$

The effects of the radiation of energy can be included in the above equations by equating the radiation reaction force $\mathbf{F}_{\text{rad}}$ to an effective electric field $\mathbf{E}_{\text{rad}} = \mathbf{F}_{\text{rad}}/e$. When a charge e accelerates under the action of a force, it radiates electromagnetic energy. This modifies the motion of the charge, which appears as if it was acted upon by an additional force—a radiation reaction force.[50] By considering the work done on the charge by the radiation and equating this to the radiated energy, an expression for the radiation reaction force is obtained,

$$\mathbf{F}_{\text{rad}} = \frac{e^2}{6\pi\varepsilon_b c^3}\ddot{\mathbf{v}}, \tag{13}$$

where $\mathbf{v}$ is the velocity of the charge and c is the speed of light. The radiation reaction force depends on the second derivative of the velocity with respect to time and involves the electric permittivity of the background ε_b.

Now consider a dipole moment $\mathbf{p} = e\mathbf{r}_0 \exp(-i\omega t)$ that oscillates with time. The position vector is $\mathbf{r} = \mathbf{r}_0 \exp(-i\omega t)$ so that the second derivative of the velocity is

$$\ddot{\mathbf{v}} = \dddot{\mathbf{r}} = i\omega^3 \mathbf{r}_0 \exp(-i\omega t) = i\omega^3 \mathbf{p}/e. \tag{14}$$

Then the radiation reaction field is

$$\mathbf{E}_{\text{rad}} = \frac{ik^3}{6\pi\varepsilon_b}\mathbf{p}, \tag{15}$$

where $k = \omega/c$ is the wave number of the radiation.

The effect of the radiation reaction force can be included in the expression for the induced resonances by adding the reaction field to the applied field $\mathbf{E}_0 + \mathbf{E}_{\text{rad}}$ in Eq. (12). This leads to an expression for the dipole moment

$$\mathbf{p} = \left(\vec{\mathbf{I}} - \frac{ik^3}{6\pi\varepsilon_b}\vec{\boldsymbol{\chi}}\right)^{-1} \cdot \vec{\boldsymbol{\chi}} \cdot \mathbf{E}_0, \tag{16}$$

which involves the unit dyadic $\vec{\mathbf{I}}$. This is the same form as that derived by Wokaun *et al.*[51] who considered the effect of radiation damping in surface-enhanced Raman scattering. After some simple algebra using Eq. (16), the expansion coefficient in Eq. (9) can be written as

$$a_q^k = \mathbf{b}_q^k \cdot \left(\vec{\mathbf{I}} - \frac{ik^3}{6\pi\varepsilon_b}\vec{\boldsymbol{\chi}}\right)^{-1} \cdot \mathbf{E}_0. \tag{17}$$

Expression (17) gives the expansion coefficient of the surface charge density induced by an applied electric field taking into account the effect of re-radiation of energy. The relative strength of the kth resonance is controlled by the factor $\mathbf{b}_q^k$ which is large for modes with a strong dipolar character [see Eq. (8)]. However, as implied by Eq. (15), this is also associated with strong radiation and therefore leads to large factors in the denominator of Eq. (17), thus limiting the near-field strength. So there is a trade-off between resonance, and therefore near-field strength, and radiation damping. The term $a_q^k\sigma_q^k(\mathbf{r})$ is invariant with changes to the overall dimensions of the particle, on account of orthogonality condition (5) and the presence of $\tau_q^k(\mathbf{r})$ in Eq. (8). However, the calculation of the dipole moment, as in Eq. (10), requires us to specify the scale or units of volume since it involves the integral of a length over a surface. This means that the radiation damping can only be determined once the absolute

size of the particle is known (i.e., the damping changes with particle size).

Given the charge distribution $\sigma(\mathbf{r})$ the electric field associated with the excitation of the particle is obtained from Coulomb's law. For any given particle, the excitation is found by solving Eq. (2) for the eigenvalues and eigenfunctions. This is conveniently done by dividing the surface of the particle into a set of discrete elements and converting the formula into a matrix product.[37] Then the solution is obtained by solving the matrix eigenvalue problem.

It is important to note that the procedure outlined in this section is not limited to a single particle, but it can easily handle an ensemble of particles. Even though the surfaces are disconnected, the solution to the eigenvalue problem still provides the resonant modes of the ensemble. However, we wish to gain some insight into the coupling between particles that leads to the resonances of the ensemble.

III. INTERPARTICLE COUPLING

It was shown in Secs. II A and II B that the excitation of a resonance is by coupling of the incident light with the surface dipole moment integrated over the particle. For particle modes where the dipole moment is zero, there is no coupling to the incident radiation, which is generally of a dipolar character. Such modes do not lose energy through dipole radiation either. The excitation of these modes can occur through the evanescent fields of nearby particles, and the modes can radiate, either through higher-order multipole radiation, or by evanescent field coupling to the nearby particles. It is of interest to determine the factors that control this coupling and of greater interest to find asymmetries in the coupling so that electromagnetic energy is preferentially coupled one way or the other.

In this section we develop the formalism for describing the coupling between an ensemble of nanoparticles, where the eigenfunctions $\sigma_q^k(\mathbf{r})$ and $\tau_q^k(\mathbf{r})$ and eigenvalues γ_q^k of each particle are known. We begin by generalizing the results of Sec. II to multiple particles and then, for completeness, include the effects of dipole radiation damping. The key result is an expression for the coupling coefficient between particles which is examined in greater detail in Sec. IV.

A. Multiparticle coupling

The electric field at position $\mathbf{r}_l$ arising from a particle j is given by Coulomb's law

$$\mathbf{E}_j(\mathbf{r}_l) = \frac{1}{4\pi\varepsilon_b}\oint \frac{(\mathbf{r}_l - \mathbf{r}_j)}{|\mathbf{r}_l - \mathbf{r}_j|^3}\sum_k a_j^k \sigma_j^k(\mathbf{r}_j)dS_j$$

$$= \oint \mathbf{g}(\mathbf{r}_l - \mathbf{r}_j)\sum_k a_j^k \sigma_j^k(\mathbf{r}_j)dS_j. \tag{18}$$

The charge distribution has been expressed as a sum over the surface charge eigenfunctions using Eq. (6) and the subscripts have been added to indicate the particle to which the parameters belong. This equation also defines a function $\mathbf{g}$ which we describe as a vector Green's function linking two points, one on each particle. The expansion coefficient is given by Eq. (7),

$$a_j^k = f_j^k \oint \tau_j^k(\mathbf{r}_j)\hat{\mathbf{n}}_j \cdot \mathbf{E}(\mathbf{r}_j)\cdot dS_j, \tag{19}$$

which is re-written to keep the field inside the integral and where the resonance factor is

$$f_j^k = \frac{(\varepsilon_j - \varepsilon_b)(\varepsilon_j^k - \varepsilon_b)}{\varepsilon_j^k - \varepsilon_j}. \tag{20}$$

The complex permittivity of the jth particle is ε_j and the real permittivity associated with the kth eigenvalue of the jth particle is ε_j^k, as would be evaluated using Eq. (3). This factor becomes large at resonance where the real part of the permittivity of the particle equals the permittivity associated with the eigenvalue. The imaginary part of ε_j, which accounts for losses in the metal, prevents Eq. (20) from becoming infinite at resonance.

The electric field at some position $\mathbf{r}_j$ on the jth particle arising from the applied field $\mathbf{E}_0(\mathbf{r}_j)$ and the electric fields from N surrounding particles is

$$\mathbf{E}(\mathbf{r}_j) = \mathbf{E}_0(\mathbf{r}_j) + \sum_{m=1}^{N} \mathbf{E}_m(\mathbf{r}_j). \tag{21}$$

In this formula, we define the electric field from the jth particle acting on itself as zero, $\mathbf{E}_j(\mathbf{r}_j) \equiv 0$. For notational convenience, let $\mathbf{E}_{jm} \equiv \mathbf{E}_m(\mathbf{r}_j)$ so that the electric field at position $\mathbf{r}_l$ arising from a particle j can be written as

$$\mathbf{E}_{lj} = \sum_k \left\{ \oint \mathbf{g}(\mathbf{r}_l - \mathbf{r}_j)\sigma_j^k(\mathbf{r}_j)dS_j \right\} \left\{ f_j^k \oint \tau_j^k(\mathbf{r}_j)\hat{\mathbf{n}}_j \cdot \left(\mathbf{E}_{j0} + \sum_{m=1}^{N} \mathbf{E}_{jm} \right) dS_j \right\}, \tag{22}$$

which combines Eqs. (18), (19), and (21). When this field acts on a particle at $\mathbf{r}_l$, it will excite a number of eigenmodes h with expansion coefficients a_l^h. To further simplify the expressions, define

$$\xi_{lj}^h \equiv f_l^h \oint \tau_l^h(\mathbf{r}_l)\hat{\mathbf{n}}_l \cdot \mathbf{E}_{lj} dS_l, \tag{23}$$

which is the expansion coefficient associated with the hth eigenfunction of the electric field at particle l arising from particle j. Then the expression for the expansion coefficient is

$$\xi_{lj}^h = \sum_k \left\{ f_l^h \oint \oint \tau_l^h(\mathbf{r}_l)\hat{\mathbf{n}}_l \cdot \mathbf{g}(\mathbf{r}_l - \mathbf{r}_j)\sigma_j^k(\mathbf{r}_j)dS_j dS_l \times \left(\xi_{j0}^k + \sum_{m=1}^{N} \xi_{jm}^k \right) \right\}. \tag{24}$$

The factor in Eq. (24) involving the Green's function represents the overlap between the surface charge eigenfunction of one particle and the surface dipole eigenfunction of the other. This is an important result as it clearly shows an asym-

metry in the coupling from one particle to another. This factor can be represented by a coupling matrix

$$C_{lj}^{hk} \equiv f_l^h \oint \oint \tau_l^h(\mathbf{r}_l)\hat{\mathbf{n}}_l \cdot \mathbf{g}(\mathbf{r}_l - \mathbf{r}_j)\sigma_j^k(\mathbf{r}_j)dS_j dS_l, \quad (25)$$

so that Eq. (24) takes on a simple form

$$\xi_{lj}^h = \sum_k C_{lj}^{hk}\xi_{j0}^k + \sum_k \sum_{m=1}^N C_{lj}^{hk}\xi_{jm}^k. \quad (26)$$

Finally, we recognize that the sum over particle numbers can also be removed by summing over j. Let $\xi_l^h \equiv \Sigma_{j=1}^N \xi_{lj}^h$ then the expression can be re-arranged in terms of the applied field

$$\sum_{j=1}^N \sum_k (\delta_{jl}\delta^{kh} - C_{lj}^{hk})\xi_j^k = \sum_{j=1}^N \sum_k C_{lj}^{hk}\xi_{j0}^k. \quad (27)$$

This is a matrix equation that can be inverted to obtain the expansion coefficients in terms of the applied field, taking into account the interactions between the particles. In the notation that has been introduced, the expansion coefficient is

$$a_j^k = f_j^k \oint \tau_j^k(\mathbf{r}_j)\hat{\mathbf{n}}_j \cdot \left(\mathbf{E}_0(\mathbf{r}_j) + \sum_{m=1}^N \mathbf{E}_m(\mathbf{r}_j)\right) \cdot dS_j = \xi_{j0}^k + \xi_j^k. \quad (28)$$

By inverting Eq. (27) the expansion coefficient is given by

$$a_j^k = \xi_{j0}^k + \sum_h \sum_{l=1}^N \sum_{m=1}^N \sum_d (\delta^{kh}\delta_{jl} - C_{lj}^{hk})^{-1} C_{lm}^{hd}\xi_{m0}^d, \quad (29)$$

where the sums over l and m are over particles and those over h and d are over the eigenfunctions. Note that $C_{jj}^{hk} \equiv 0$, which follows from our definition that the electric field from particle j acting on itself is zero. For a large number of particles, the analytic evaluation of Eq. (29) is complicated by the need to invert the matrix involving the coupling coefficient. However, computationally it is straightforward to evaluate, involving only sums over the particles and knowledge of the geometry, eigenmodes, and relative positions.

From Eq. (25) the important parameters that determine the coupling between particles are the resonance strength of the particle, the surface dipole distribution of the particle, the surface charge distribution of the other particle, the distance between the particles, and finally the relative orientation of one particle in relation to the other, expressed though the unit normal. The ramifications of this will be examined in Sec. IV. However, for completeness we conclude this section by including the effect of radiation damping into the formalism.

B. Radiation damping with multiparticle coupling

Up to this point we have neglected radiation damping. However, this is important as it will affect the resonances associated with particle ensembles and it will be useful to obtain an analytical expression for it in terms of the interparticle coupling. In this section we confine our discussion to dipole radiation which can be included in the multiple particle interaction in a straightforward manner. We combine a radiation dipole term with the electric fields acting on a particle and carry through with the derivation as in Sec. II. The dipole term analogous to Eq. (23) is

$$p_j^k \equiv f_j^k \oint \tau_j^k(\mathbf{r}_j)\hat{\mathbf{n}}_j \cdot \mathbf{p}_j dS_j, \quad (30)$$

where $\mathbf{p}_j$ is the dipole moment of particle j. The expansion coefficient [Eq. (29)] becomes

$$a_j^k = \xi_{j0}^k + i\alpha p_j^k + \sum_h \sum_{l=1}^N \sum_{m=1}^N \sum_d (\delta^{kh}\delta_{jl} - C_{lj}^{hk})^{-1} \times C_{lm}^{hd}(\xi_{m0}^d + i\alpha p_m^d), \quad (31)$$

where $\alpha = k^3/6\pi\varepsilon_b$.

By defining another matrix

$$M_{jn}^{kd} = \delta_{jn}\delta^{kd} + \sum_h \sum_{l=1}^N (\delta^{kh}\delta_{jl} - C_{lj}^{hk})^{-1} C_{lm}^{hd}, \quad (32)$$

this expression can be written more compactly as

$$a_j^k = \sum_{m=1}^N \sum_d M_{jm}^{kd}(\xi_{m0}^d + i\alpha p_m^d). \quad (33)$$

To solve this equation, the induced dipole moment is expressed in terms of the expansion coefficient so that

$$\mathbf{p}_j = \sum_k a_j^k \mathbf{p}_j^k. \quad (34)$$

By using Eq. (33) and rearranging for $\mathbf{p}_j$ we have

$$\mathbf{p}_j = \sum_{m=1}^N \sum_d \sum_k \mathbf{p}_j^k M_{jm}^{kd} \mathbf{b}_m^d \cdot (\mathbf{E}_{m0} + i\alpha \mathbf{p}_m) = \sum_{m=1}^N \vec{\boldsymbol{\chi}}_{jm} \cdot (\mathbf{E}_{m0} + i\alpha \mathbf{p}_m), \quad (35)$$

where we have introduced the matrix dyadic

$$\vec{\boldsymbol{\chi}}_{jm} = \sum_d \sum_k \mathbf{p}_j^k M_{jm}^{kd} \mathbf{b}_m^d. \quad (36)$$

Again, Eq. (35) is in the form of a matrix equation. Its solution can be written in the form

$$\mathbf{p}_m = \sum_j \sum_n (\vec{\mathbf{I}}\delta_{jm} - i\alpha\vec{\boldsymbol{\chi}}_{jm})^{-1} \vec{\boldsymbol{\chi}}_{jn} \cdot \mathbf{E}_{n0}. \quad (37)$$

When substituted into Eq. (30) and the result combined with Eq. (33) the expansion coefficient is given by

$$a_j^k = \sum_{m=1}^N \sum_d M_{jm}^{kd} \mathbf{b}_m^d \cdot \sum_{n=1}^N (\vec{\mathbf{I}}\delta_{nm} - i\alpha\vec{\boldsymbol{\chi}}_{nm})^{-1} \cdot \mathbf{E}_{n0}, \quad (38)$$

which can be used to determine the electric field strength arising from a particle and its dependence on radiation losses for multiple particles.

IV. COUPLING BETWEEN PARTICLE PAIRS

The coupling coefficient [Eq. (25)] and the surface charge expansion coefficient [Eq. (29)] play important roles in determining the excitation of nanoparticle resonances by an applied electric field and by the evanescent fields from nearby particles. The expressions are complicated by allowing for the excitation of multiple particles and many different modes. To examine the features of these expressions, the problem is greatly simplified by considering just two particles and assuming that the incident electric field is at a frequency that excites only one eigenmode within each particle. This is often the case when the frequency of the incident electric field is close to a resonance of the particle. We shall assign the subscripts 1 and 2 to the two particles and, since each particle is associated with a unique eigenmode, we omit the separate labels for the modes. For simplicity, radiation damping will be neglected in the first instance. With reference to Eq. (29), in matrix form we have the coupling coefficient

$$C_{lm}^{hd} \to \begin{bmatrix} 0 & C_{12} \\ C_{21} & 0 \end{bmatrix}, \tag{39}$$

and

$$(\delta^{kh}\delta_{jl} - C_{lj}^{hk})^{-1} \to \begin{bmatrix} 1 & -C_{12} \\ -C_{21} & 1 \end{bmatrix}^{-1} = \frac{1}{1 - C_{12}C_{21}} \begin{bmatrix} 1 & C_{12} \\ C_{21} & 1 \end{bmatrix}, \tag{40}$$

so that the amplitudes are

$$\begin{bmatrix} a_1 \\ a_2 \end{bmatrix} = \begin{bmatrix} \xi_{10} \\ \xi_{20} \end{bmatrix} + \frac{1}{1 - C_{12}C_{21}} \begin{bmatrix} C_{12}C_{21} & C_{12} \\ C_{21} & C_{21}C_{12} \end{bmatrix} \begin{bmatrix} \xi_{10} \\ \xi_{20} \end{bmatrix}. \tag{41}$$

The terms in the matrix have a simple interpretation. The factor C_{12} represents the coupling of the field from particle 2 to particle 1. The factor $C_{12}C_{21}$ represents the coupling from particle 1 to 2 and then back from 2 to 1. Explicitly

$$a_1 = \frac{\xi_{10} + C_{12}\xi_{20}}{1 - C_{12}C_{21}}, \tag{42}$$

and

$$a_2 = \frac{\xi_{20} + C_{21}\xi_{10}}{1 - C_{12}C_{21}}. \tag{43}$$

The coupling coefficients, and therefore the surface charges and associated electric fields, become large when the real part of the denominator in Eq. (42) or (43) is zero. This factor is the determinant associated with the matrix inverse [Eq. (40)] and it controls the resonance of the particle pair. However, the far-field dipole radiation of the pair of particles depends on their combined dipole moments, which depends on the relative signs of the coupling coefficients. In the following sections we consider the effect of coupling on the resonance frequencies and on the evanescent fields. As we show, this leads to a situation where a particle pair can exhibit a collective dark mode.

A. Resonance splitting

The proximity of resonant particles to one another leads to coupling through their induced electric fields which alters their resonant frequencies. This effect has been used in the "plasmon ruler" to measure the distance between particles optically.[52,53] The resonances are obtained from the condition that the determinant in Eq. (40) is zero. The resonance condition is easily found by re-writing the coupling coefficient to show explicitly the dependence on the electric permittivity. Let $C_{12}=(\varepsilon-\varepsilon_b)\eta_{12}/(\varepsilon_1-\varepsilon)$, where ε_1 is the permittivity associated with eigenvalue γ_1 through Eq. (3), and similarly for C_{21}. Then the condition for a resonance takes the form

$$(\varepsilon_1 - \varepsilon)(\varepsilon_2 - \varepsilon) - \eta_{12}\eta_{21}(\varepsilon - \varepsilon_b)^2 = 0. \tag{44}$$

As this equation is quadratic, we see that it can have two solutions for the particle permittivity ε required for the pair to resonate, which varies depending on the degree of coupling between the particles. Define $\varepsilon_{12}^{av} \equiv (\varepsilon_2+\varepsilon_1)/2$ to be the average of the eigenvalue permittivities for the two particles and $\Delta\varepsilon_{21} \equiv (\varepsilon_2-\varepsilon_1)/2$ as half the difference, then the particle permittivity is given by

$$\varepsilon = \frac{\varepsilon_{12}^{av} - \eta_{12}\eta_{21}\varepsilon_b}{1 - \eta_{12}\eta_{21}} \pm \frac{[(1 - \eta_{12}\eta_{21})\Delta\varepsilon_{21}^2 + \eta_{12}\eta_{21}(\varepsilon_{12}^{av} - \varepsilon_b)^2]^{1/2}}{1 - \eta_{12}\eta_{21}}, \tag{45}$$

which solves for the real part of the electric permittivity. For no coupling Eq. (45) gives two solutions for the permittivity that correspond to the resonances of the individual particles. The coupling leads to a shift in these resonant frequencies. For identical particles with the same resonant frequency, the two solutions represent a splitting of this resonance into two separate frequencies.

An estimate of the effect on the surface charges of the resonance splitting can be obtained from Eqs. (42) and (43) by assuming we have two particles that are almost identical so that their surface charge eigenfunctions $\sigma_1 \approx \sigma_2 = \sigma_p$ and the coupling of the incident field $\xi_{10} \approx \xi_{20} = \xi$ are approximately the same. Furthermore, let there be a small difference in their coupling coefficients so that $C_{12} \approx C(1+\delta)$ and $C_{21} \approx C(1-\delta)$, where δ is taken only to first order. The surface charge induced on each particle is determined to first order in δ by the amplitudes

$$a_1 \approx \xi(1 + C + C\delta)/(1 - C^2) \tag{46}$$

and

$$a_2 \approx \xi(1 + C - C\delta)/(1 - C^2), \tag{47}$$

and the total surface charge of the pair of particles is given by

$$\sigma = (a_1 + a_2)\sigma_p \approx 2\sigma_p\xi/(1 - C). \tag{48}$$

At resonance there are two possible values for the coupling coefficient. For $C=1$ there is a strong resonance for the particle system, where, to first order, the denominators in Eqs. (46)–(48) are zero. (For this discussion we ignore the imaginary part of the resonance factor.) The surface charges in-

TABLE I. The dimensions of the stripes used in the simulations and the first eigenvalue. The resonance wavelength associated with the eigenvalue corresponds to a gold stripe embedded in a material with a permittivity of $\varepsilon_b=2.2$ (e.g., PMMA). The units are arbitrary as only the aspect ratios are important in the electrostatic approximation.

Shape	Length	Width	Thickness	No. triangles	Fundamental eigenvalue and wavelength
1	270	100	40	496	1.1423 (925.1 nm)
2	300	100	40	560	1.1233 (978.6 nm)

duced on both particles are in phase and sum to give a large resonant response, which is a symmetric resonance mode. This corresponds to the smaller permittivity in Eq. (45) and a shorter wavelength (blueshifted) resonance. However when $C=-1$ the combined system has a very weak resonance since the denominator in Eq. (48) remains finite. But examination of Eqs. (46) and (47) shows that the individual amplitudes a_1 and a_2 are large and have opposite signs indicating an antisymmetric resonance mode. Moreover, since the combined response is weak, this mode will have a small dipole moment and low scattering of radiation. This is a dark mode. The strength of the fields in this mode is controlled by the fractional difference δ between the coupling coefficients.

The splitting and the associated modes can be calculated using the numerical procedures outlined by Mayergoyz and colleagues[37–39] based on a two-particle system of metal stripes. The stripe system was chosen as it can be reproduced using lithographic means enabling an experimental test of the theory. The geometry of the stripes is given in Table I. For numerical implementation, the surfaces were tessellated with triangles as shown in Fig. 1. The coupling between them is controlled by varying their separation.

Eigenvalue problem (3) was solved for the two stripes individually yielding the eigenvalues, surface charge, and surface dipole eigenfunctions needed to evaluate the coupling coefficients. The electric permittivities as functions of

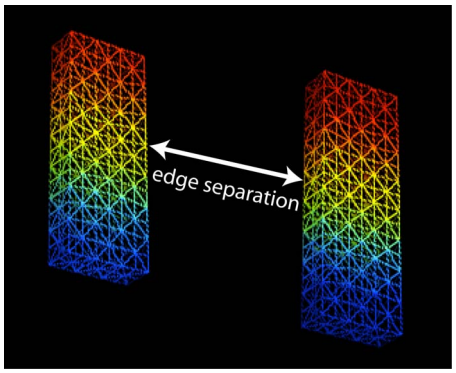

FIG. 1. (Color online) This shows the triangle tessellation of the two numerical stripes used to model the coupling. The color (online version) represents the surface dipole distribution associated with the first resonance of each individual stripe, where blue is positive and red is negative.

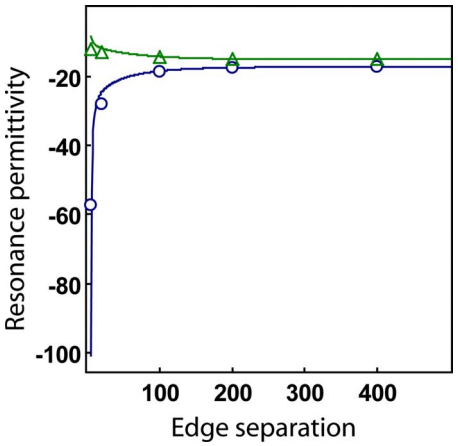

FIG. 2. (Color online) The permittivity associated with the resonance of the two-particle (stripes) system, based on Eq. (45) as a function of the separation of the stripes. The permittivities calculated from the eigenvalues of the coupled system are shown for the low-frequency (circles) and high-frequency (triangles) modes.

edge-to-edge separation (Fig. 1) of the two stripes were calculated using Eq. (45) and the results are shown in Fig. 2. There are two branches corresponding to the two modes for this pair of particles. In addition, by treating the separated stripes as elements of a single system, we can solve eigenvalue problem (3) for the ensemble and deduce the permittivities associated with resonances from the eigenvalues using Eq. (4) with $\varepsilon_b=1$. These are shown as the points in the figure for the two lowest eigenvalues $\gamma>1$. There is good agreement between the two methods, as would be expected, except at very small separations. In particular, the high-frequency (smaller permittivity) mode begins to deviate significantly from Eq. (45) which is due to significant coupling from the higher-order modes. In this case the assumption that only one mode in each stripe is significant is breaking down.

A measure of the interaction of incident light with the two stripes is given by the cross section for dipole scattering[54]

$$C_{sca}=\frac{k^4}{6\pi}\left|\frac{\mathbf{p}}{E_0}\right|^2, \tag{49}$$

where $\mathbf{p}$ is the dipole moment of the ensemble of stripes. The scattering cross section is shown in Fig. 3, normalized to the

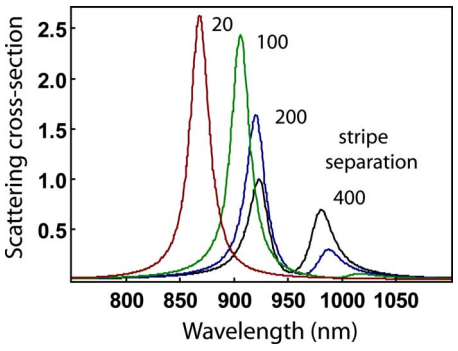

FIG. 3. (Color online) The scattering cross section (arbitrary units) for the two stripe system for four different separations. The stripes were taken to be gold embedded in PMMA.

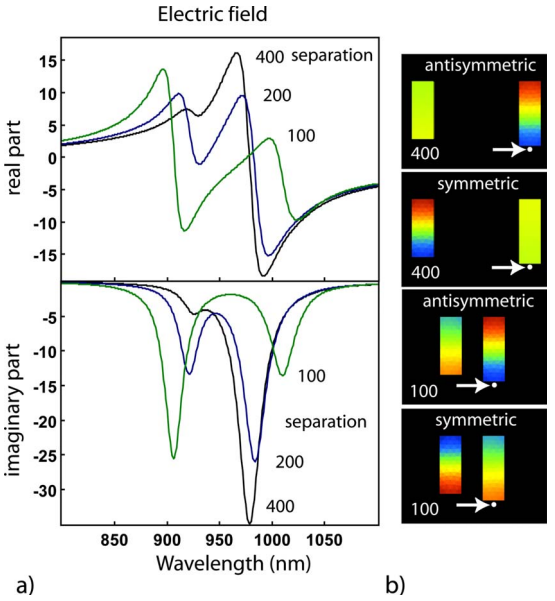

FIG. 4. (Color online) (a) The real and imaginary parts of the component of the electric field parallel to the long axes of the stripes. The field is calculated at a point 10 units from the long axis of the longer stripe. The imaginary component indicates the wavelength where the coupled stripes resonate. Note the significant electric fields at 1010 nm even though the scattering cross section at this wavelength is small. The stripes were taken to be gold embedded in PMMA. (b) The surface dipole distributions for two modes when the stripes are far apart (400) and close (100): the arrow indicates the point where the electric field is calculated.

short-wavelength resonance for the two stripes when separated by 400 units. As discussed above, the higher-frequency (shorter wavelength) resonance becomes blueshifted as the separation of the two stripes is reduced. The lower frequency (longer wavelength) resonance is redshifted but it is also significantly diminished in strength, indicating a reduction in the scattering from the pair of stripes. For the 20 unit separation the lower-frequency cross section is very small and is redshifted to 1220 nm.

The component of the induced electric field parallel to the long axes of the stripes at a point 10 units from one end of the larger stripe is shown as a function of wavelength in Fig. 4. The incident electric field was chosen with unit amplitude and a polarization parallel to the long axes of the stripes. The striking feature of these data is the strong electric field at 1010 nm corresponding to a separation of 100 units, even though the scattering cross section is very small at this wavelength. This simple system, consisting of two stripes with slightly different resonances, exhibits a strong electric field but very little scattering, corresponding to the formation of a dark mode. The slight length difference between the two stripes creates an asymmetry that results in a small residual dipole moment for the pair. The external electric field couples to the stripes through this residual dipole moment. This general trend is consistent with the simple analysis given above.

B. Radiation damping and dark modes

It is of interest to examine the radiation damping associated with this system and the effect on the dark mode. For this calculation we need to specify a scale for the stripes, as discussed in Sec. II. In Fig. 5 we reproduce the scattering cross section for the particle without radiation damping and include the cross sections when the scale is chosen so that the longer stripe is 100 and 150 nm long. The cross sections have been normalized to bring their maxima to the same value. Also in this figure is the component of the induced electric field parallel to the long axes of the stripes, calculated at a point 10 units beyond the long axis of the longer stripe. The radiation damping increases with the size of the stripes. The effect of radiation damping is to broaden and reduce the scattering cross section associated with the symmetric mode at 900 nm but has little effect on the asymmetric mode at 1010 nm. The electric fields associated with the symmetric mode are significantly reduced by the damping. The interesting feature is that this is not true for the asymmetric dark mode. There has only been a small decrease in the field strength with radiation damping because the dipole moment of the pair of stripes is small, due to the asymmetry of the mode. The radiation damping depends on the dipole moment which is suppressed in this configuration. More importantly, for larger stripes the electric fields of the dark

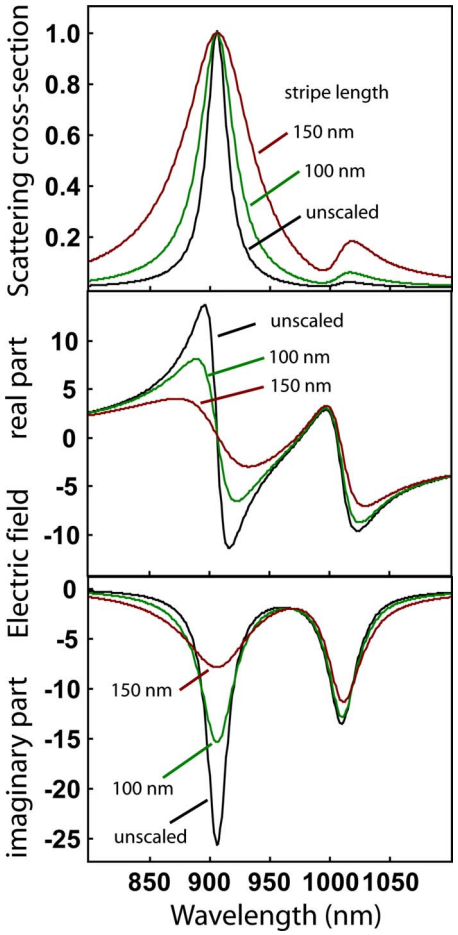

FIG. 5. (Color online) The effect of radiation damping on the scattering cross section of a pair of stripes (gold embedded in PMMA) and on the electric field component 10 units beyond the long axis of the longer stripe. The scales refer to the length of the longer stripe. The radiation damping varies with the size scale whereas the unscaled stripe has no radiation damping.

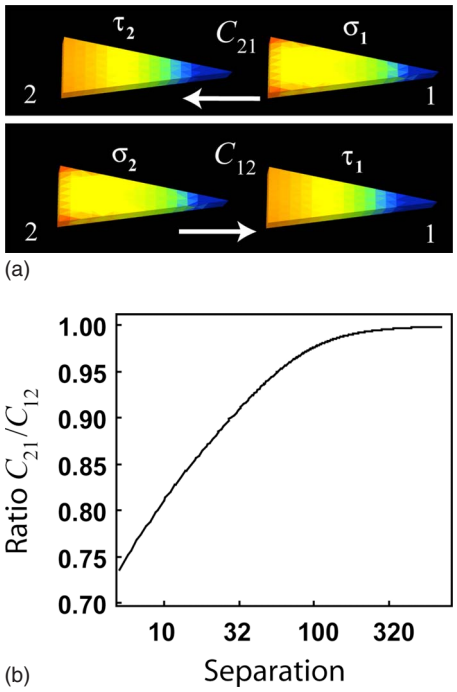

FIG. 6. (Color online) The asymmetry in coupling coefficients associated with identical asymmetric particles. (a) the triangular prisms showing the surface charge σ and surface dipole τ eigenmodes, the coupling coefficients, and the "direction" of the coupling. (b) a graph of the coupling ratio vs separation between the prisms, demonstrating the asymmetry.

mode are stronger than the symmetric mode and the widths of the resonances are narrower.

C. Orientation dependence and asymmetry

The coupling between particles depends not only on the modes excited within each particle, but also on the geometry of one particle relative to the other (for example, Fig. 6). Referring to Eq. (25), the coupling is simply the integrated response of the individual couplings between the surface charge $\sigma_j^k(\mathbf{r}_j)$ at a point $\mathbf{r}_j$ on the surface of particle j and the surface dipole moment $\tau_l^h(\mathbf{r}_l)\hat{\mathbf{n}}_l$ at a point $\mathbf{r}_l$ on the surface of particle l. The coupling is mediated through the electric field arising from the surface charge at each point of particle j. The field has a direction given by $(\mathbf{r}_l-\mathbf{r}_j)/|\mathbf{r}_l-\mathbf{r}_j|$ but it is only the component of this field parallel to the surface normal $\hat{\mathbf{n}}_l$ at $\mathbf{r}_l$ on particle l that is important. The surface dipole and surface charge eigenfunctions for the same mode are similar in form but are not identical. This means that for two particles j and l that are not identical, the coupling from particle j to particle l is likely to be different from the reverse coupling, from particle l to particle j. This is due to the different characteristics of the surface charge and surface dipole distributions over the respective particles with the result that $C_{lj} \neq C_{jl}$. In addition to this, there are shape- and geometry-dependent terms that can introduce an asymmetry, which comes about through the dependence of the coupling on the direction vector from the surface of particle j to particle l in relation to the surface normal of particle l. The relative orientation of one particle to another is also important in this respect.

As an example of asymmetry, the coupling between two identical triangular prisms as a function of displacement is shown in Fig. 6. In this model the prisms are identical, being 300 units long, 100 units across at the base, and tessellated with 560 surface elements. The eigenvalue for the fundamental mode is $\gamma=1.0740$. Figure 6(a) shows the two coupling directions, the surface charge, and surface dipole distributions. The arrows point from the surface charge of one prism, in the direction of the coupling, to the other prism which shows the surface dipole distribution. Note how the surface charges tend to accumulate at the sharp points, a well-known property of electric charge, whereas the surface dipoles are more evenly distributed. The ratio of the coupling coefficients is shown in Fig. 6(b) as a function of separation between the prisms. As expected, the coefficients are different and this becomes more pronounced as the particles approach one another. The dominant terms in the integral of Eq. (25) for the coupling coefficient occur for the closest points between each prism. These points lie along the base of prism 1, which has its surface normal directed toward prism 2, but they lie along sides of prism 2 that lead to is apex. These sides have surface normals almost at right angles (80.5°) to the direction of prism 1. This means that the coupling C_{21} will be smaller than C_{12}, on account of the $\hat{\mathbf{n}}_2.(\mathbf{r}_2-\mathbf{r}_1)$ term. This asymmetry should become more pronounced as the prisms approach one another, and this is born out in Fig. 6(b).

V. CONCLUSION

In this paper we have derived analytical formulas that describe the interactions between arbitrary numbers of metallic nanoparticles in the electrostatic approximation. The key result is a description of the coupling coefficients that contain explicitly the effects of the electric field from one particle acting on the surface dipoles of another and shows the relationship between the geometry, surface modes, and the localized surface-plasmon resonances of the particles. In addition we included the effects of radiation damping into the formalism, which is important when optimizing the resonances and the strengths of the electric fields. Some of the features of the method were demonstrated with a two-particle system consisting of gold stripes embedded in PMMA (polymethylmethacrylate), as could be formed using lithographic methods. By restricting each of the particles to single resonant modes, the coupling matrix is easily written down and solved. It was shown how the coupling between particles leads to changes in the resonances of the ensemble and how this leads to two different resonant modes. The asymmetric mode was associated with a dark mode and it was demonstrated that it has markedly reduced scattering, low radiation damping, and large electric fields. The analytical form of the coupling coefficients shows an inherent asymmetry in the coupling and this was demonstrated with an example of the coupling between triangular prisms.

While we have concentrated on two-particle coupling, it is straightforward to write down and solve the matrix for

three particles, provided each is restricted to a single mode. This leads to more complex interactions and greater freedom in designing structures with the desired electromagnetic properties. This will be investigated in future publications. In general, this work can be used for an arbitrary number of interacting particles and should lead to a further understanding of the stimulation of dark mode structures, the enhancement of near-fields through particle interaction, design of SERS substrates, plasmon solar cells, and the design of highly sensitive plasmon-based sensors.

[1] A. W. Clark, A. K. Sheridan, A. Glidle, D. R. S. Cumming, and J. M. Cooper, Appl. Phys. Lett. **91**, 093109 (2007).
[2] C. Dahmen and G. von Plessen, Aust. J. Chem. **60**, 447 (2007).
[3] P. K. Jain and M. A. El-Sayed, Nano Lett. **8**, 4347 (2008).
[4] D. A. Schultz, Curr. Opin. Biotechnol. **14**, 13 (2003).
[5] S. Lal, S. Link, and N. J. Halas, Nat. Photonics **1**, 641 (2007).
[6] J. J. Mock, D. R. Smith, and S. Schultz, Nano Lett. **3**, 485 (2003).
[7] A. Rai, M. Chaudhary, A. Ahmad, S. Bhargava, and M. Sastry, Mater. Res. Bull. **42**, 1212 (2007).
[8] M. J. Banholzer, J. E. Millstone, L. Qin, and C. A. Mirkin, Chem. Soc. Rev. **37**, 885 (2008).
[9] R. J. C. Brown and M. J. T. Milton, J. Raman Spectrosc. **39**, 1313 (2008).
[10] E. Hao and G. C. Schatz, J. Chem. Phys. **120**, 357 (2004).
[11] T. Jensen, L. Kelly, A. Lazarides, and G. C. Schatz, J. Cluster Sci. **10**, 295 (1999).
[12] J. P. Kottmann, O. J. F. Martin, D. R. Smith, and S. Schultz, Chem. Phys. Lett. **341**, 1 (2001).
[13] S. Lal, N. K. Grady, J. Kundu, C. S. Levin, J. B. Lassiter, and N. J. Halas, Chem. Soc. Rev. **37**, 898 (2008).
[14] J. J. Mock, M. Barbic, D. R. Smith, D. A. Schultz, and S. Schultz, J. Chem. Phys. **116**, 6755 (2002).
[15] N. P. W. Pieczonka and R. F. Aroca, Chem. Soc. Rev. **37**, 946 (2008).
[16] M. I. Stockman, Phys. Rev. Lett. **93**, 137404 (2004).
[17] M. I. Stockman, S. V. Faleev, and D. J. Bergman, Phys. Rev. Lett. **87**, 167401 (2001).
[18] K. Yamaguchi, T. Inoue, M. Fujii, M. Haraguchi, T. Okamoto, M. Fukui, S. Seki, and S. Tagawa, Chin. Phys. Lett. **24**, 2934 (2007).
[19] S. Zou and G. C. Schatz, Chem. Phys. Lett. **403**, 62 (2005).
[20] J. P. Kottmann and O. J. F. Martin, Phys. Rev. B **64**, 235402 (2001).
[21] C. Hagglund, M. Zach, G. Petersson, and B. Kasemo, Appl. Phys. Lett. **92**, 053110 (2008).
[22] H. Li, R. H. Franken, R. L. Stolk, J. A. Schauttauf, C. H. M. van der Werf, J. K. Rath, and R. E. I. Schropp, J. Non-Cryst. Solids **354**, 2445 (2008).
[23] A. J. Morfa, K. L. Rowlen, T. H. Reilley III, M. J. Romero, and J. van de Lagemaat, Appl. Phys. Lett. **92**, 013504 (2008).
[24] S. Pillai, K. R. Catchpole, T. Trupke, and M. A. Green, J. Appl. Phys. **101**, 093105 (2007).
[25] B. P. Rand, P. Peumans, and S. R. Forrest, J. Appl. Phys. **96**, 7519 (2004).
[26] A. Yakimov and S. R. Forrest, Appl. Phys. Lett. **80**, 1667 (2002).
[27] N. A. Issa and R. Guckenberger, Opt. Express **15**, 12131 (2007).
[28] C. Ropers, C. C. Neacsu, T. Elsaesser, M. Albrecht, M. B. Raschke, and C. Lienau, Nano Lett. **7**, 2784 (2007).
[29] S. Zhang, D. A. Genov, Y. Wang, M. Liu, and X. Zhang, Phys. Rev. Lett. **101**, 047401 (2008).
[30] S. E. Harris, Phys. Today **50** (7), 36 (1997).
[31] A. Alu and N. Engheta, Opt. Express **15**, 7578 (2007).
[32] K. J. Boller, A. Imamoglu, and S. E. Harris, Phys. Rev. Lett. **66**, 2593 (1991).
[33] M. Fleischhauer, A. Imamoglu, and J. P. Marangos, Rev. Mod. Phys. **77**, 633 (2005).
[34] J. Li and C. Z. Ning, Phys. Rev. Lett. **93**, 087402 (2004).
[35] D. McGloin, D. J. Fulton, and M. H. Dunn, Opt. Commun. **190**, 221 (2001).
[36] C. Rohde, K. Hasegawa, and M. Deutsch, Opt. Lett. **32**, 415 (2007).
[37] I. D. Mayergoyz, D. R. Fredkin, and Z. Zhang, Phys. Rev. B **72**, 155412 (2005).
[38] I. D. Mayergoyz and Z. Zhang, IEEE Trans. Magn. **43**, 1681 (2007).
[39] I. D. Mayergoyz, Z. Zhang, and G. Miano, Phys. Rev. Lett. **98**, 147401 (2007).
[40] F. J. García de Abajo and A. Howie, Phys. Rev. B **65**, 115418 (2002).
[41] J. Liaw, Eng. Anal. Boundary Elem. **30**, 734 (2006).
[42] V. Myroshnychenko, J. Rodríguez-Fernández, I. Pastoriza-Santos, A. M. Funston, C. Novo, P. Mulvaney, L. M. Liz-Marzán, and F. J. García de Abajo, Chem. Soc. Rev. **37**, 1792 (2008).
[43] F. J. García de Abajo and A. Howie, Phys. Rev. Lett. **80**, 5180 (1998).
[44] T. V. Teperik and F. J. García de Abajo, V. V. Popov, and M. S. Shur, Appl. Phys. Lett. **90**, 251910 (2007).
[45] I. Romero, J. Aizpurua, G. W. Bryant, and F. J. García de Abajo, Opt. Express **14**, 9988 (2006).
[46] H. Xu and M. Käll, Phys. Rev. Lett. **89**, 246802 (2002).
[47] R. Quidant, A. S. Zelenina, and M. Nieto-Vesperinas, Appl. Phys. A **89**, 233 (2007).
[48] R. Quidant and C. Girard, Laser Photonics Rev. **2**, 47 (2008).
[49] F. J. García de Abajo, Phys. Rev. B **60**, 6086 (1999).
[50] J. D. Jackson, *Classical Electrodynamics*, 2nd ed. (Wiley, Sydney, 1975).
[51] A. Wokaun, J. P. Gordon, and P. F. Liao, Phys. Rev. Lett. **48**, 957 (1982).
[52] B. M. Reinhard, M. Siu, H. Agarwal, A. P. Alivisatos, and J. Liphardt, Nano Lett. **5**, 2246 (2005).
[53] P. K. Jain, W. Huang, and M. A. El-Sayed, Nano Lett. **7**, 2080 (2007).
[54] C. F. Bohren and D. R. Huffman, *Absorption and Scattering of Light by Small Particles* (Wiley, Sydney, 1983).